


Article

A Wavelet-Based Diagnostic Framework for CRD Engine Injection Systems under Emulsified Fuel Conditions

Ugochukwu Ejike Akpudo  and Jang-Wook Hur *

Department of Mechanical Engineering (Department of Aeronautics, Mechanical and Electronic Convergence Engineering), Kumoh National Institute of Technology, 61 Daehak-ro (yangho-dong), Gumi 39177, Korea; akpudougo@gmail.com

* Correspondence: hhjw88@kumoh.ac.kr

Abstract: The impact of the constituent oxides of nitrogen, carbon, sulphur, and other particulate matter which make up the gas emissions from diesel engines has motivated several control techniques for these pollutants. Water-in-diesel emulsions provide a reliable solution, but the wear effects on the fuel injection system (FIS) still pose remarkable concerns. Because pressure signals from the common rail (CR) reflect the dynamics associated with varying emulsion compositions and at varying engine RPMs, an investigative (and diagnostic) study was conducted on a KIA Sorento 2004 four-cylinder line engine at various water-in-diesel emulsion compositions and engine speeds. Alongside visual/microscopic inspections and spectral analyses, the diagnostic framework proposed herein functions on the use of standardized first-order differentials of the CR pressure signals to generate reliable continuous wavelet coefficients (CWCs) which capture discriminative spectral and transient information for accurate diagnosis. The results show that by extracting the CWCs from the first-order CR pressure differentials up to the 512th scale on a Mexican hat wavelet, adequate fault parameters can be extracted for use by a deep neural network (DNN) whose hyperparameters were globally optimized following a grid search. With a test accuracy of 92.3% against other widely-used ML-based diagnostic tools, the proposed DNN-based diagnostics tool was empirically assessed using several performance evaluation metrics.

Keywords: wavelet transform; CRD engine; water-emulsified diesel; damage severity; fuel injection system; fault detection and isolation; spectral analysis



check for updates

Citation: Akpudo, U.E.; Hur, J.-W. A Wavelet-Based Diagnostic Framework for CRD Engine Injection Systems under Emulsified Fuel Conditions. *Electronics* **2021**, *10*, 2922. <https://doi.org/10.3390/electronics10232922>

Academic Editor: Ahmad Taher Azar

Received: 11 October 2021

Accepted: 24 November 2021

Published: 25 November 2021

Publisher's Note: MDPI stays neutral with regard to jurisdictional claims in published maps and institutional affiliations.



Copyright: © 2021 by the authors. Licensee MDPI, Basel, Switzerland. This article is an open access article distributed under the terms and conditions of the Creative Commons Attribution (CC BY) license (<https://creativecommons.org/licenses/by/4.0/>).

1. Introduction

Over the years, diesel engines have become a major power source for industrial and personal use. In contrast to gasoline fuel engines, the high thermal efficiency, cost efficiency, and durability of diesel fuel engines are some of the advantages associated with them; however, the inherent emissions contribute significantly to air and water pollution with the constituents nitrogen oxides (NO_x), particulate matter (PM), and carbon monoxide (CO) being primarily responsible for greenhouse effects and a wide array of human health and environmental concerns [1,2]. Notwithstanding obvious environmental concerns, diesel engines require scheduled (or predictive) maintenance schemes for ensuring optimum engine performance and minimizing pollution from exhaust emissions [3]. On a global scale, it is estimated that diesel emissions constitute about 30% of greenhouse emissions and have ignited public concerns for alternative energy sources, including biodiesel and renewable energy sources [1]. These alternatives are projected to replace combustible energy sources soon; however, the resources required for the imminent switch are yet to be fully harnessed on a global scale while the increasing energy demand remains. As Kalghatgi [4] showed in his study, a 75% increase in energy demand for commercial transportation is expected in 2040 with the highest demand for diesel expected to come from the Asia-Pacific and European regions.

The FIS of a CRD engine is designed to function ideally with clean diesel and high-quality components, but the fact remains that the publicly available diesel fuels are not 100% pure, hence the need for regular engine maintenance and fuel quality monitoring. Furthermore, the recent hike in fuel price accompanied by strict emission regulations has provided valid research motivations for diesel emulsification in various compositions for improving fuel quality, reducing emission severity, and minimizing costs [5–8]. Invariably, the need for emission control, improving diesel fuel efficiency, and extending the useful lifetime of engines have long motivated several improvement techniques. Among the diverse techniques available, diesel emulsification (in the right composition) has shown to improve the chemical properties of diesel fuels which in turn minimizes the quantity of pollution-causing agents that include nitrogen oxides (NO_x), particulate matter (PM), and carbon monoxide (CO) [9]. The water in emulsified diesel fuel induces micro-explosions to form many small-sized emulsion droplets that enhance mixing. This process invariably minimizes NO_x, CO, and PM emissions [10]. On the other hand, excessive emulsion compositions may have adverse effects on the FIS and the engine at large; therefore, it is necessary to employ reliable condition monitoring and diagnostic methodologies for maintaining optimum engine performance on water-in-diesel (W/D) emulsified fuels [3].

Because the FIS of a CRD engine is the heart of the engine, a deviation from the ideal fuel composition and running condition would reflect in the CR system. The information provided by the CR system provides diagnostic parameters needed for condition monitoring, fault detection and isolation (FDI), and accurate failure diagnosis [11]. As a result, several techniques have been reported in the past for diesel engine CR systems (and injectors) FDI and are broadly classified into model-based, data-driven, and hybrid methods [12]; nonetheless, these methods aim to identify faulty operating conditions or localize faults using intelligent and/or statistical techniques. On the bright side, recent studies show a strong steer from purely physics-of-failure (PoF) methods towards the artificial intelligence (AI)-based methods which learn and map the linear and complex dependencies from input parameters for predicting target conditions [13,14]. To achieve these, numerous time-domain, frequency-domain, time-frequency-domain, and bio-inspired signal processing methods abound for feature extraction, and with fusion techniques, multi-domain methods can be achieved in a comprehensive framework for diversified representation [15]. On the flip-side, the curse of dimensionality and feature redundancy opens up an even greater opportunity for the filter-based, wrapper-based, and hybrid feature selection methods to flourish. These selection methods aim to isolate only highly discriminative diagnostic parameters to achieve accurate cost-efficient diagnostic performance and minimize classifier confusion [15,16]. Notwithstanding the approach employed, identification of key diagnostic parameters from the inputs (CR signals) for reliable diagnosis is critical, and this has provided the leeway for this study.

The remainder of this paper is structured as follows: Section 2 discusses some related works to CRD characteristics and diagnosis, while Section 3 presents the materials and methods employed in this study. Section 4 presents the experimental results and discussion, while Section 5 concludes the paper.

2. Motivation and Literature Review on Related Works

W/D emulsion fuels have proven in many studies to improve the chemical properties of diesel fuel and minimize the pollution-causing effects from engine emissions [17]. This is because the presence of water in emulsified fuels causes micro-explosions that enhance fuel quality. When exposed to high temperature, emulsion droplets undergo preferential evaporation, triggering puffing and micro-explosion to form several smaller-sized droplets that enhance mixing. This invariably reduces NO_x, CO, and PM emissions [10]. These benefits associated with diesel emulsification have motivated several investigative studies for verification and possible recommendations. For instance, Senthur et al. [18] conducted diverse experiments for finding the right substitute fuel(s) to diesel by preparing different W/D emulsions and using them for comparing emission performance and combustion

parameters in conventional CRD engines. Their results reveal that increased W/D emulsion correlates with diminished emission parameters with the best meeting point at 15% water content. In conclusion, the study validates the superiority of W/D emulsion over conventional diesel. Similarly, Fahd et al. [19] compared the efficiency of a 10% W/D emulsion with conventional diesel by evaluating the engine exhaust gas performance under changing engine speed conditions. Their findings revealed that even though the engine efficiency was reduced under the 10% W/D emulsion (in comparison with pure diesel), at higher engine speeds, the engine efficiency under the emulsified fuel condition was similar to when pure diesel fuel was used. In addition, a higher brake-specific fuel consumption (BSFC) (accompanied with a reduction in exhaust gas temperature) was observed at all rotation speeds [19]. Other studies [20,21] also validate the benefits associated with diesel emulsification, yet the high oxidation potential of water on metal components means that W/D emulsion adoption still poses strong concerns [22].

The increasing demand for emission reduction in the automotive industry has motivated manufacturers on directing their innovative solutions towards achieving higher power densities from mass-produced automotive diesel engines [23,24]. Although most of the recent efforts (in simulated environments) are geared towards realizing lower compression ratio combustion systems, engine downsizing (to minimize engine emissions), enhancing the air charging system efficiencies, designing FISs capable of more than 2700 bar, and optimizing/controlling operating parameters at these higher FIS outputs [25–27], actualizing them is still open to further investigations considering that these innovative solutions focus on maintaining (rather than reducing) engine emission levels on a global scale. With the corrosion/wear effect on engine components parts by W/D emulsion fuels, meeting such high-power design expectations may take some time [28–30]. Although available studies reveal encouraging paradigms for the use of water-emulsified diesel fuels, the reliability of such methods remains open for continued discussions. Issues of stability, mixing conditions, temperature, and mixing compositions greatly influence the reliability of water-emulsified diesel fuels [28,31]. Most studies suggest the use of surfactants to enhance emulsion fuel stability and physio-chemical properties, yet their efficiency still depends on achieving appropriate hydrophilic–lipophilic balance (HLB) value [31]. Consequently, these phenomena have motivated several research studies on the quest for proper condition monitoring techniques for emulsified diesel fuel engines using the CR system [1,3,4,9,11]. By leveraging the vulnerabilities of CR systems to emulsified fuels, reliable condition monitoring frameworks can be developed. This shall help ensure a safe emulsion composition is maintained for retaining acceptable engine efficiencies. Krogerus and Huhtala [1] explored a signal filtering and normalization technique of CR pressure signals for determining a fault/failure threshold of the CR system. Their results showed that the derivative of the filtered signals provides reliable diagnostics characteristics, and they are suitable for injection duration identification. Song [11] proposed the use of an improved variational mode decomposition (VMD) processing algorithm and hierarchical dispersion entropy on CR pressure signals for achieving a time-series condition monitoring on water-emulsified high-pressure diesel engines. Above the efficiencies of traditional statistical-based diagnostics schemes, the reliability of these methods is limited by expensive statistical assumptions and trade-offs during the modeling process [12,13].

On-going research suggests the use of bio-inspired mathematical models with deep architecture—traditional machine learning (ML) and deep learning (DL) methods—for optimal diagnostic performance; however, identifying the key diagnostic parameters from CR signals (inputs) remains open for continued studies. Beyond the limitations of traditional machine learning techniques such as random forests and decision trees, DL methods such as convolutional neural networks (CNN), recurrent neural networks (RNN), etc., are designed for large-scale systems designed with big data and demand for automated performance with little/no domain knowledge; however, the inherent issues of interpretability, high dependence on excessive parameters, overfitting/underfitting, need for high computational power, feature evaluation complexity, and their magical defiance from fundamental

statistical principles often raise strong concerns for cost-aware and safety-critical applications [12,32–34]. Particularly, due to the high stochasticity and complexity in their learning process, feature evaluation/selection (from an empirical perspective) is often limited; hence, this limits the explainability of the diagnostic model(s) based on feature importance/impact. On the other hand, although they demand a significant amount of domain knowledge, several established time-frequency-domain signal processing/feature extraction methods are available for use. These tools, including wavelet transform (WT), empirical mode decomposition (EMD), Mel frequency spectral coefficients (MFCC), short-time Fourier transform (STFT), etc., provide dependable avenues for identifying key diagnostic parameters [15], and with appropriate feature selection/dimensionality reduction techniques, salient feature selection can be achieved for optimum diagnostic results. Against the limitations of these methods, continuous wavelet transform (CWT) has superior efficiencies for non-stationary signal processing; however, its efficiency depends on the choice of mother wavelet [15]. Notwithstanding, the Shannon entropy of the corresponding wavelet coefficients provides an efficient criteria for choosing the befitting mother wavelets when rightly extracted. These coefficients invariably can be used as reliable diagnostics parameters on an ML-based classifier for diagnosis [15,35,36]. In our quest for investigating the characteristics of CR fluctuations in a W/D emulsion fuel using CR pressure signals, this study makes the following contributions:

- An investigative study was conducted on the CR system of a KIA Sorento 2004 diesel engine operating on varying W/D emulsion compositions and engine speeds. The effect and damage severity of W/D emulsion fuels on critical FIS components were explored, presented, and via a degradation/wear assessment, empirical judgements were made on the correlations between fuel conditions and engine performance.
- A DNN-based diagnostic scheme is proposed for condition monitoring which exploits the rail pressure sensor (RPS) signals by a wavelet-based signal processing technique. Against the poor efficacies of the raw RPS signals, their first-order differential provides standardized inputs for CWC extraction which provide discriminative inputs for DNN-based classification.
- Extensive descriptive and empirical conclusions are drawn. The research results are expected to provide a modern paradigm for condition monitoring, failure diagnostics, design, and decision-making for CRD engines with W/D emulsion fuels.

3. Background of Study

This section presents in detail the background of a typical FIS, the test engine and preparation procedure, and the diagnostic methodology employed in this study.

3.1. Common Rail Injection System

Typically, the CR injection system consists of a high-pressure pump (HPP), CR pipe, fuel injector, and electronic control unit (ECU). Figure 1 illustrates these components and the fuel/energy flow directions whereby the blue lines indicate a low-pressure fluid flow, while the red lines indicate a high-pressure fluid flow.

As illustrated in Figure 1 in yellow, from the reservoir, the low-pressure pump delivers fuel through a filter to the HPP which then delivers fuel at high pressure through the CR pipe to the CR. Some high-pressure CR system configurations may contain a restrictor valve/pressure control valve (PCV) between the CR pipe outlet and the fuel injector accumulator chamber. The throttling effect of the PCV helps curtail abnormal fuel flow in the CR pipe; however, as illustrated in red in Figure 1, an ideal injection process entails a flow through the CR pipe, to the accumulator of the injector, and the injector body before being injected into the cylinder. The ECU controls the opening and closing of the injector. Every time fuel is injected into the cylinder, an instant pressure drop is witnessed in the CR pipe, but this is immediately compensated by the HPP and its regulator.

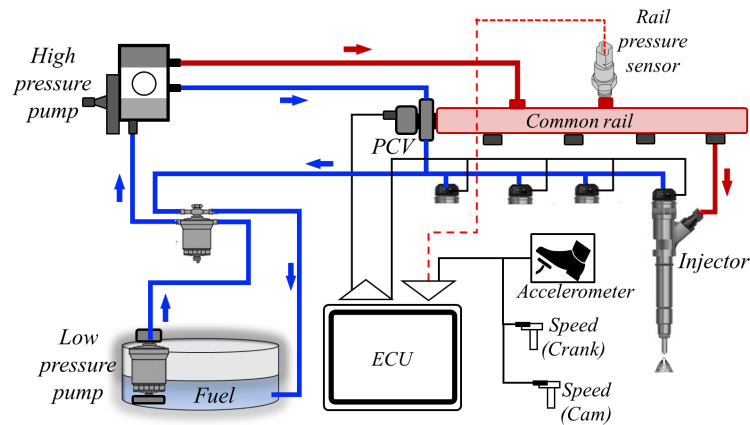


Figure 1. A typical common rail diesel fuel injection system.

These fluctuations in pressure are captured by the rail pressure sensor—a transmitter for capturing and storing the pressure measurements digitally for analysis and condition monitoring. The accelerator pedal, when pressed down, decreases the injection duration, thereby increasing the combustion process to generate more engine power. As shown in Figure 1, the whole process is controlled by the ECU.

3.2. Test Engine and Fuels

To investigate the proposed study, a KIA Sorento 2004 four-cylinder line engine (passenger car), whose specification is detailed in Table 1, was used to acquire experimental data.

Table 1. Test engine specifications.

| Car Model | Engine Type | Bore × Stroke (mm) | Maximum Power | Maximum Torque (Nm/RPM) | Compression Ratio | Fuel Injection | Aspiration |
|------------------|-------------------|--------------------|-------------------|-------------------------|-------------------|----------------|----------------------------|
| KIA Sorento 2004 | In-line, Four (4) | 91 × 96 | 138 hp @ 3800 RPM | 343 Nm @ 1900 RPM | 17.6 | Common Rail | Turbocharged, inter-cooled |

The experiment was conducted as shown in Figure 2 in the following manner: first, different water compositions are mixed with petroleum diesel to form different emulsion compositions represented as “EM-x%” (where x represents the water concentration by volume in (100 – x)% of diesel. For instance, EM-5% contains 5% of water and 95% of diesel. First, the car’s fuel tank was isolated and an external custom reservoir was designed for the experiment. To avoid phase separation, the water-emulsified fuels were constantly stirred by an overhead stirrer (OSA-10 made by LK LABKOREA, Namyangju-si, Korea) and tested for stability with a centrifuge.

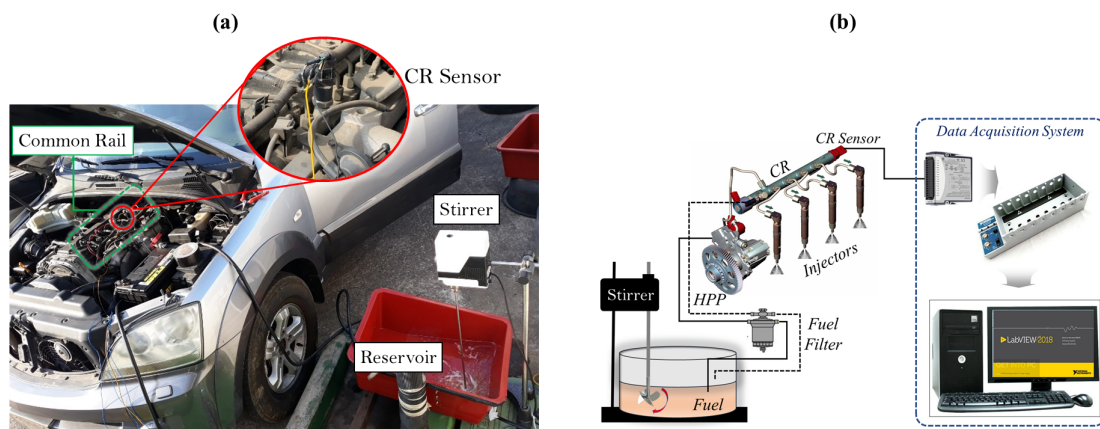


Figure 2. A view of (a) the actual experiment setup, (b) schematic view of the experimental setup.

As shown in Figure 2b, the pressure signals were collected from the pressure sensor via an NI 9228 at 200 Hz sampling rate via the engine’s rail pressure sensor (RPS)–Bosch 0 281 002 405 via a NI 9228 module (connected to a NI cDAQ 9178 and LabView software) produced by National Instruments CORP. The RPS outputs a maximum of $(5 \pm 0.25)V$ at 2200 bar with a response time $(\tau_{10/90}) \leq 5mSecs$ and a maximum overpressure of 1800 bar (rupture pressure = 3000 bar). Alongside the pressure signals, the real-time engine temperature data were also collected via NI 9214 module at 1 KHz with an RTD thermocouple affixed to the exhaust manifold.

Before data collection for the operating conditions (emulsion composition and varying engine speeds), the engine is allowed to run smoothly for at least 30 min to ensure an even distribution of the particular emulsion composition through the injection system. Moreover, this ensures that the engine temperature for the particular temperature is stable. To collect data for another operating condition, the engine is flushed for at least 1 h with the emulsion composition of interest.

3.3. Proposed Diagnostic Method

RPS signals are usually non-stationary due to the fluctuations from the PCV and varying engine speeds (from the accelerator control), and this demands the use of non-stationary signal processing techniques for identifying characteristic (and fault) parameters. On the one hand, since these pressure signals are influenced by the periodic fuel injection from the injector, as proposed in [1], extracting the time-dependent derivatives of the CR signals not only helps to better identify injection duration, but also to identify fault characteristic parameters from the signal. On the other hand, choosing a befitting mother wavelet for extracting CWCs from a signal remains one of the inhibiting factors for employing wavelet transforms; however, because the level of similarity between a wavelet is directly proportional to the corresponding energy concentration, they provide reliable paradigms for mother wavelet selection. Figure 3 shows the diagnostic pipeline employed in this study.

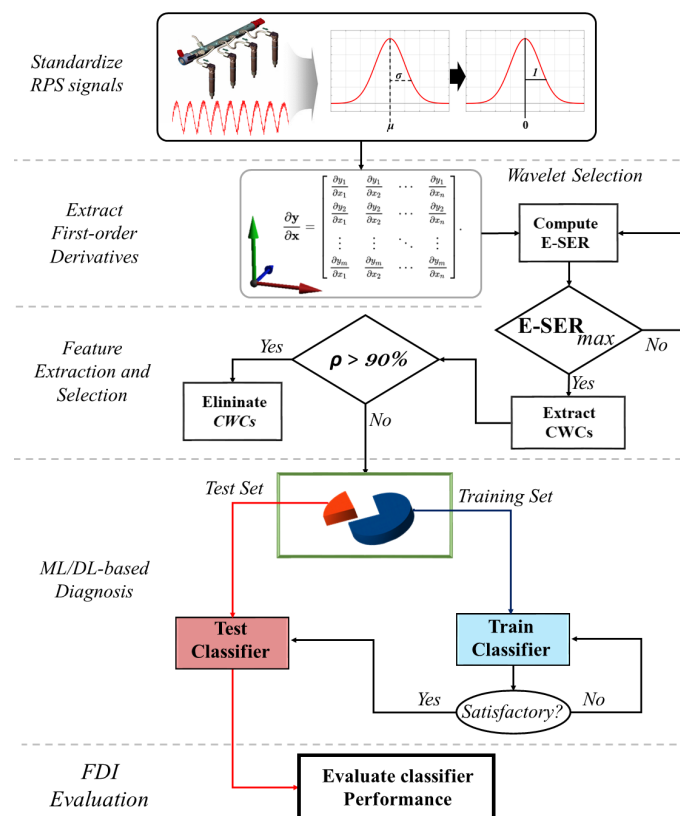


Figure 3. Proposed diagnostic pipeline.

As shown in Figure 3, the model initiates by standardizing the raw RPS signals to improve the stationarity and discriminance of the inputs. Given the raw CR signals $a(t) = \{a(t)_1, a(t)_2, \dots, a(t)_N\}$, the standardized outputs are computed using Equation (1):

$$x(t)_i = \frac{a(t)_i - \mu}{\sigma} \quad (1)$$

where μ and σ represent the mean and the standard deviation of $a(t)$, respectively.

This is then followed by extracting the first-order derivatives of the standardized signals using Equation (2)

$$x'(t)_i = \frac{x(t_{i+1}) - x(t_{i-1}))}{2 * \Delta t} \quad (2)$$

3.3.1. Diagnostic Feature Extraction and Selection

Motivated by the robustness of the wavelet transform for time-frequency-domain signal processing, the computed differentials are further processed for feature extraction. The wavelet transform represents a signal in the form of wavelet series—a representation of a square-integrable (real or complex-valued) function by a certain non-orthogonal series generated by a wavelet [15,35,36]. Unlike the Fourier transform-based methods (STFT, MFCC, etc.), this robust technique projects a signal into wavelets which invariably offer better localization in the frequency domain and provide more reliable spectral (and transient) information for diagnostics.

Given the finite energy differentials $x'(t)$, the wavelet transform $WT(a, b)$ is the convolution of $x'(t)$, with a scale and conjugated wavelet $\psi(t)$, as shown in Equation (3).

$$WT(a, b) = \frac{1}{\sqrt{a}} \int_{-\infty}^{\infty} x'(t) \psi(t)^* \left(\frac{t-b}{a} \right) dt \quad (3)$$

where $\psi(t)^*$ is the complex conjugate of the single function $\psi_{a,b}(t)$ obtained by translation and dilation of the mother wavelet $\psi(t)$, as shown in Equation (4).

$$\psi_{a,b}(t) = \frac{1}{\sqrt{a}} \psi \left(\frac{t-b}{a} \right) \quad (4)$$

where a is the scaling parameter ($a > 0$), b is the localization parameter ($b \in R$) and $|1/\sqrt{a}|$ is a normalization factor for energy preservation.

Although reliably efficient, choosing the befitting mother wavelet becomes a challenge; nevertheless, a befitting wavelet is expected to extract the maximum amount of energy while minimizing the Shannon entropy of the corresponding wavelet coefficients [37]. Consequently, the energy–Shannon entropy ratio (E-SER) defined in Equation (5) provides an efficient paradigm for choosing the right wavelet.

$$E - SER(j) = \frac{E(j)}{S_{\text{entropy}}(j)} \quad (5)$$

where $E(j)$ and $S_{\text{entropy}}(j)$ are the energy wavelet coefficients and Shannon entropy at j th scale, respectively. They are obtained by Equations (6) and (7), respectively:

$$E(j) = \sum_{k=1}^k |WT(j, k)|^2 \quad (6)$$

$$S_{\text{entropy}}(j) = - \sum_{k=1}^k p_k \log_a p_k \quad (7)$$

where k is the total number of wavelet coefficients, $WT(j, k)$ is the k -th wavelet coefficient of j scale, and p_k is the energy probability distribution of wavelet coefficients. Consequently, by using non-orthogonal wavelets, the outputs—continuous wavelet coefficients (CWCs)—

can be used as fault features/parameters since they capture both transient and spectral information.

Quite often, not all features are optimally useful for diagnostic problems, and as the number of classes increase beyond binary cases, the need for salient feature extraction increases. Although there are numerous filter-based, wrapper-based, and hybrid methods available for exploration, as a pre-processing step, the Pearson's correlation filter-based techniques provides a reliable, cost-efficient, and unsupervised (unbiased) solution for salient feature selection, dimensionality reduction (to mitigate the curse of dimensionality), and avoidance of classifier confusion for diagnostics [32,38]. In this context, this step ensures that only highly uncorrelated CWCs are retained, while the highly correlated CWCs are eliminated by comparing their p-values; however, being a statistical approach which functions on the basis of a threshold for elimination/retention, the choice of an optimal threshold remains. Nonetheless, a high threshold (at least 90%) offers a very generous paradigm whereby only the highly correlated CWCs (above 90% correlation) are eliminated.

3.3.2. ML/DL-Based Diagnosis

The predominance of AI across most disciplines has motivated the high discrimination against the traditional statistical model-based approaches for FDI. Theoretically, DL methods are quite popular for high detection accuracy; however, issues of interpretability, high dependence on excessive parameters, overfitting/underfitting issues, computational cost (and complexity), and the magical defiance from fundamental statistical theory make them practically unreliable for cost-aware industrial applications [12,32–34]. On the other hand, most Bayesian ML methods come with benefits ranging from ease-of-use, interpretability, and computational efficiency on few data and provide reliable diagnostic results when provided with the right input—fault parameters/features.

In the quest for methodology generalization of ML algorithms for classification, a recent study by the authors of [37] provides an intuitive paradigm for the choice of (and discrimination against) ML classifiers for FDI. Although the results therein favored the random forest (RF) against the other classifiers including *k*-nearest neighbor (KNN), gradient-boosting classifier, (GBC) support vector machines (SVM), decision tree (DT), etc., the deduction remains questionable considering that: the features used for the comparison may be insufficient/inadequate, the study lacks a reliable parametrization paradigm for the classifiers which may result in over-fitting and/or under-fitting, issues, and the impact of discriminative feature selection was not considered. Clearly, each of these methods has their unique architecture and parameterization methods; however, from a global perspective, minus the less optimal random selection of parameters, other reliable methods including the exhaustive search, meta-heuristic optimization, and grid search methods exist for optimal parameter search.

On the brighter side, against the limitations of the other traditional ML-based algorithms, the MLP preserves superior potentials of improvement to form a DNN. For better learning, a typical MLP can be improved to form a DNN by increasing the number of hidden layers to two (2) or more hidden layers [32], and with appropriate optimization methods, its diagnostic/prognostic efficiencies can further be enhanced. The automatic (supervised) learning process of DNN (or MLP) is done via a backward propagation of weights by gradient descent (following a forward propagation process). This provides the avenue for error minimization between the predicted and actual outputs. To achieve this cost minimization, several weight optimization algorithms exist including the quasi-Newton methods [39], Adam [40], stochastic gradient descent (SGD) [41,42]; and the popular SGD improvement—the Adam [40] weight optimizer. While the SGD serves fairly for most problems and the quasi-Newton methods are popularly efficient on small datasets, the Adam optimizer comes with faster convergence, faster learning, and improved validation accuracy for large datasets.

In this study, to ensure an in-depth comparative analysis of the classifiers, the grid search technique was employed on each algorithm since the meta-heuristic techniques come with higher computational costs and extra modeling processes which require extra parametrization in addition to the diagnostic model. On the other hand, different activation functions—Tanh, recurrent linear units (ReLU), Sigmoid, and SoftMax—were explored for each of the DNN and MLP architectures designed.

3.3.3. FDI Performance Evaluation

For evaluating the diagnostic capabilities of the proposed diagnostic scheme, visual, spectral, and empirical investigations are conducted alongside popular diagnostic evaluation metrics. These metrics—confusion matrix, test accuracy, sensitivity, etc.—provide a strong paradigm for evaluating the classifier's efficiency for diagnosis. A detailed explanation of these metrics can be found in [36].

4. Experimental Results

Primarily, the major goal of the test was to understand the CR characteristics at varying W/D emulsion compositions at varying engine speeds and more in-depth results/analyses found in [21]. Overall, the investigation results revealed that as the water composition is increased in the different W/D emulsions, exhaust temperature is reduced at lower engine speeds and the viscosity increased proportionally, and this induced some wear (as a result of oxidation) on the critical FIS components—injector valve ball seats, injector nozzle needles, and injector valve pistons. Moreover, the spectral analysis presented therein suggests that a fatal adverse effect on the FIS may be observed for W/D emulsions beyond 10% composition of water. Figures A1–A3 (Appendix A) present the damage severity comparison between healthy and worn FIS components as a result of diesel emulsification.

4.1. Signal Processing and Feature Extraction

At the end of the experiment, the RPS signals for the various W/D emulsion conditions were cleaned, standardized, and processed (following the first-order differential process). Figure 4a shows a view of standardized RPS measurements acquired for the respective W/D emulsion conditions (across the rows in unique colors) at the increasing engine speeds (down the columns), respectively, while Figure 4b shows their corresponding first-order differentials.

Figure 4a reveals the high non-stationarity of the signals across the respective emulsion and speed conditions; however, as Figure 4b shows, the non-stationarity is significantly reduced by computing the first-order differentials. As observed, the differentials are stationary with zero mean values across the conditions. This better represents the signals for online/offline diagnostics purposes and ensures unbiasedness in their distributions. Furthermore, the respective wave-forms in Figure 4b are observed to be unique across each emulsion composition (and engine speed), which invariably ushers in a soft landing for the wavelet transform to flourish.

To extract the CWCs from these differentials, the suitable mother wavelet was selected by searching exhaustively amongst the non-orthogonal mother wavelets for the befitting wavelet (with maximum E-SER). Consequently, the CWCs were extracted up to the 512th scale on a Mexican hat wavelet from the training dataset which contains most of the CR pressure signals from the experiment. By so doing, both high- and low-frequency components can be captured along the time-dependent differentials, thereby ensuring a more comprehensive spectral and transient representation of the signals. Figure 5 presents the wavelet spectra (CWCs) from the first-order differentials in Figure 4b.

As shown, not only are the frequency (scale) components captured, but their respective transient fluctuations are also captured, thereby providing a reliable feature set for ML/DL-based feature learning for diagnostics. A closer observation of the spectra reveals the underlying CR dynamics of each W/D emulsion composition at different speeds (represented by varying color maps). The superior advantage of the wavelet transform for

time-frequency representation of the signals is reflected by the different scales (with diverse magnitudes) over increasing speeds. More obviously, the impact of diesel emulsification is observed at engine idling conditions (the first figure in the left of each row) by the appearance of high-magnitude scales at every 50th scale. Interestingly, our suspicion of the engine’s FIS fault at EM-10% emulsion in Figure 5f (at 2000 RPM) and beyond (all engine speeds at EM-10% emulsion) is confirmed by the numerous magnitudes in virtually all the scales in Figure 5g.

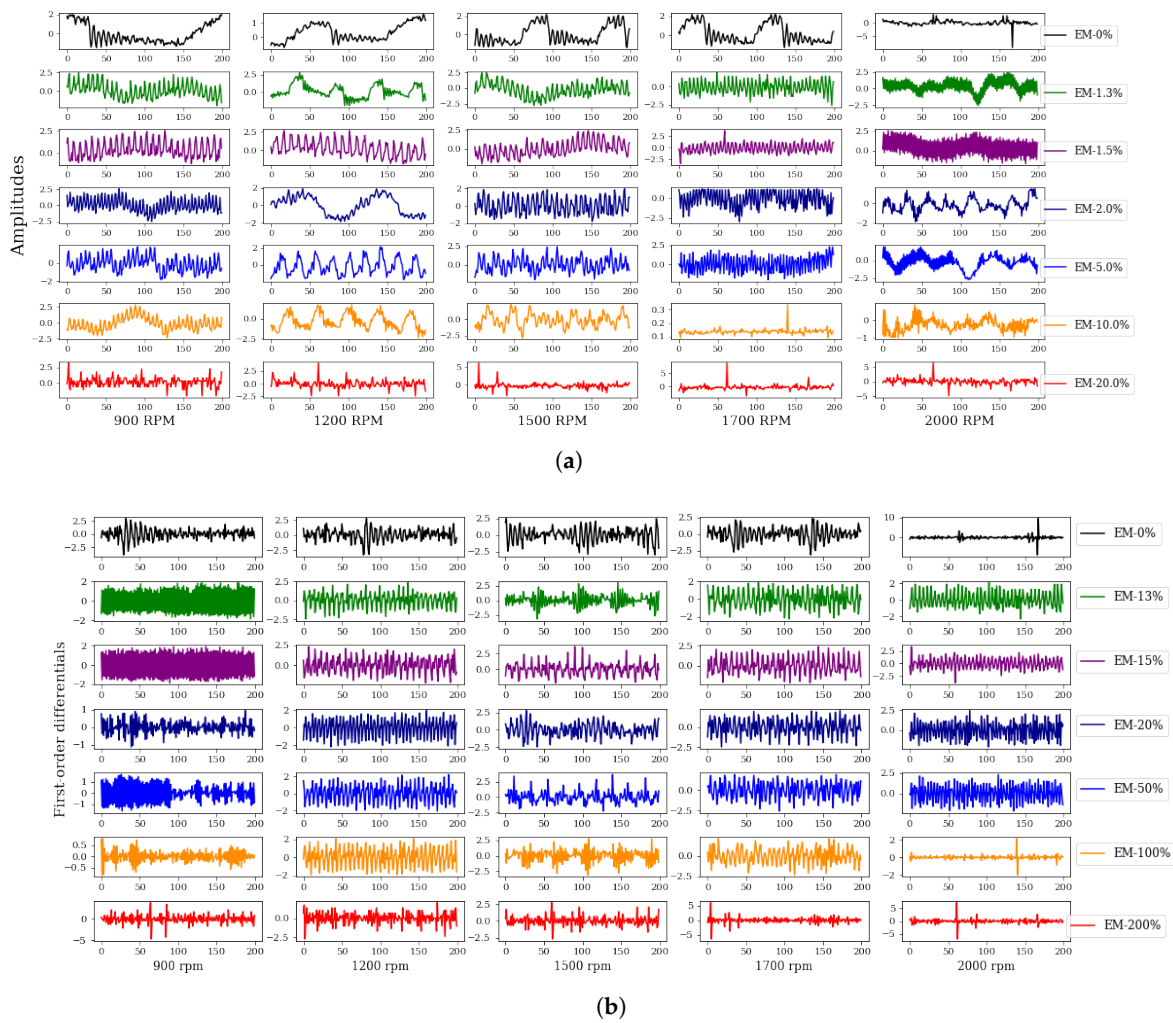


Figure 4. Visualization for (a) CR signals for different W/D emulsions (across the rows in unique colors) at the increasing engine speeds (down the columns). (b) The normalized first-order differentials of the CR pressure signals at different emulsion compositions.

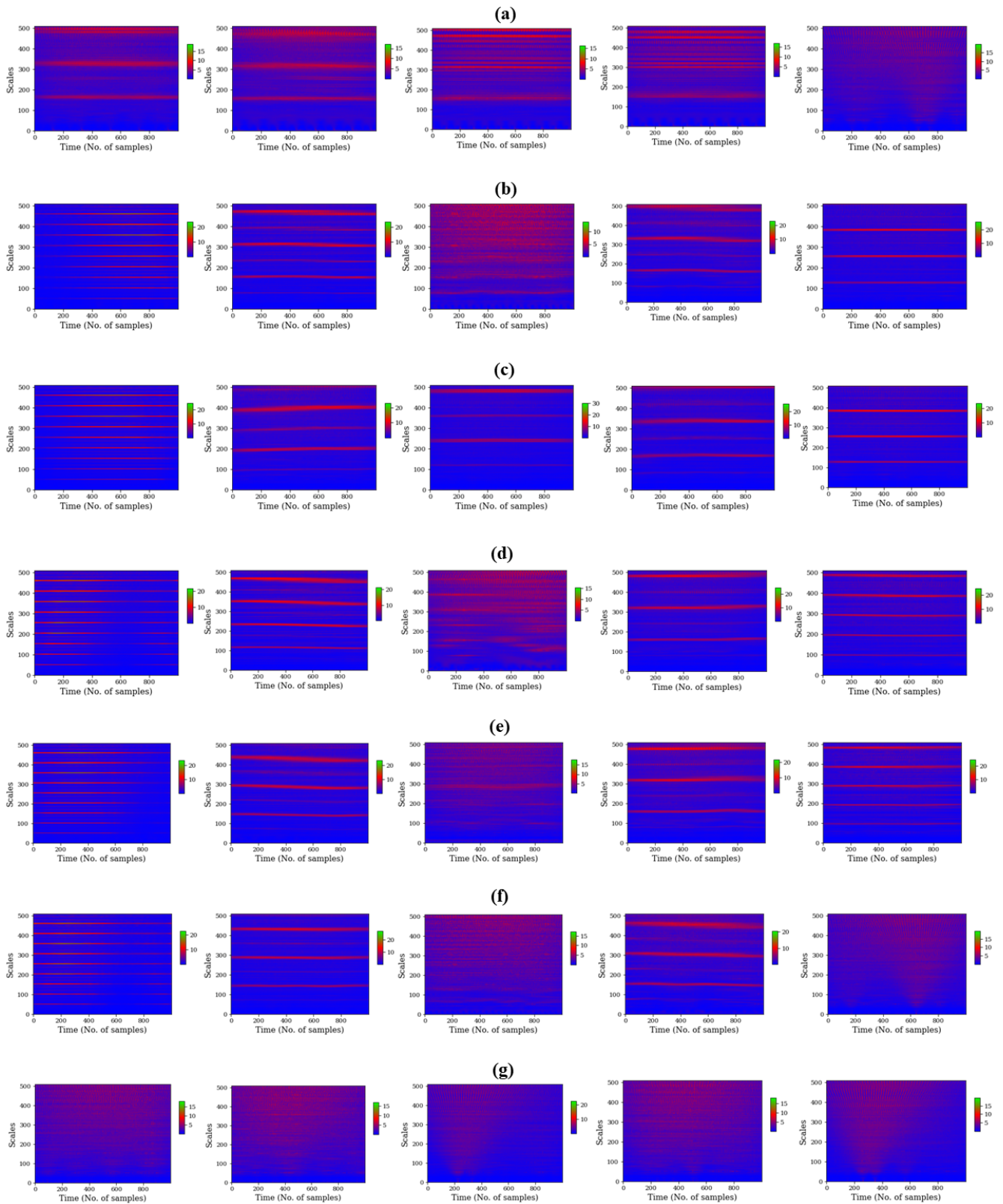


Figure 5. Wavelet spectra of the first-order differential of CR pressure signals for different emulsion compositions and increasing engine speeds (from left to right: 900, 1200, 1700, 1500, 2000 RPMs). (a) EM-0%, (b) EM-1.3%, (c) EM-1.5%, (d) EM-2.0%, (e) EM-5.0%, (f) EM-10.0%, and (g) EM-20.0%.

4.2. ML/DL-Based Diagnosis

Next, the CWCs in the training dataset are labeled respectively in the range $\{0, 1, \dots, 6\}$, representing the respective emulsion compositions. In addition, the test dataset was also prepared with a similar approach and preserved for validation of the proposed diagnostic method.

The MLP retains its robustness for multi-class problems, and with nonlinear activation functions in its architecture, reliable unsupervised feature learning/testing can be achieved after a supervised training process. Furthermore, as this study would later validate, stacking two or more MLPs to form a DNN has even better predictive accuracies for diagnosis with marginal additional computational costs. Consequently, different DNN and MLP architectures with various parameters were designed from which the best performing architecture is chosen from a grid search for optimal parameters after a five-fold cross validation. More emphatically, considering that the study entails a seven (7) class diagnostic problem statement, each of the designed DNN and MLP architectures in Table 2 has seven neurons in the input and output nodes, respectively, for accepting the extracted features—CWCs—as inputs, while the hidden layers (and numbers of neurons per layer) are varied based on Table 2.

Contrary to the MLP and DNN architecture, the learning rules of the other ML-based classifiers are respectively unique. To avoid digression, it would be futile to discuss their respective theoretical backgrounds in this study; however, for each of the ML-based classifiers employed in this study, a five-fold cross validation process was implemented to ensure that the optimal performances were recorded during performance evaluation. Following an exhaustive process, the algorithm-specific parameters summarized in Table 2 were respectively achieved for each of the classifiers and were respectively trained using the salient CWCs for comparative performance evaluation with the DNN and MLP classifiers.

As shown, each classifier is unique to their parameterization, which requires domain knowledge; however, the grid search algorithm provided an extensive and comprehensive avenue for discovering each classifier's best-performing parameters to avoid unbiased comparative assessments. Invariably, the different sets' respective parameters uniquely produce different classifiers of varying diagnostic capabilities; however, a grid search provides an avenue for evaluating their individual performances. Ideally, increasing the number of hidden layers of an MLP (to form DNN) beyond three (3) usually leads to over-fitting and computational cost inflation. It should be noted that the motivation behind the choice of the grid space values was purely based on prior experience in the domain since it would be futile to assess all the possible combinations of all integers (number of nodes) for all possible architectures (number of layers).

The grid search results on the DNN and MLP architectures summarized in Table 2 are presented in Figure 6 which show the validation scores (using 20% of the training data) over 100 epochs/iterations with 20 mini batches per epoch. An adaptive learning and Adam weight optimizer were employed considering the large amount of the dataset.

The results above reveal the validation scores of the 960 different (DNN and MLP) architectures (15 DNN Architectures each having 64 unique parameter instances) over a five-fold validation process for 50 iterations/epochs, as shown in Figure 6a. Particularly, the DNN architecture with three hidden layers with (35, 70, 14) neurons in the hidden layers returned the highest mean validation score of 98.06%. Its accompanying parameters are a ReLU activation function, an Adam weight optimizer, and a constant learning rate of 0.001. On a different note, the overall comparison of each of the 15 DNN architecture's performance are presented as box-plots. For each architecture, Figure 6b presents the median (in red) of each architecture's validation scores. As the boxplots show, not only are the DNNs (multiple layers) more accurate in comparison with the MLPs (single layer), but particularly, the DNN with three hidden layers with (35, 70, 14) neurons in the hidden layers returned the highest median validation score of 90%. This suggests that even with different parameters (activation functions and regularization parameters), the DNN architecture is quite reliable. Overall, it is observed that for the DNNs, higher validation scores are

achieved. It is also observed that as the number of layers in the hidden layer decreases, the validation scores also decrease. In sharp contrast to the DNNs, the MLPs returned the least validation scores. The MLP architecture with 70 neurons in its single hidden layer returned the highest validation score (amongst the MLPs) of 96.7%— a comparatively lower score, but reliable nonetheless.

Table 2. Optimal parameters for classifiers.

| Algorithm | Dependent Parameter | Grid Search Space | Best Grid Values |
|---------------------------------------|--|--|--|
| RF | Estimators (n) Maximum depth (m) | $n = \{10, 20, \dots 200\}$ $m = \{10, 20, \dots 100\}$ | $n = 120$ $m = 30$ |
| Logistic regression (LR) | Regularization strength inverse (C) | $C = \{0.001, 0.01, 0.1, 1, 10, 100, 1000\}$ | $C = 10$ |
| GBC | Estimators (n) Maximum depth (m) Learning rate (α) | $n = \{100, 200, \dots 1000\}$ $m = \{10, 20, \dots 100\}$ $\alpha = \{0.0001, 0.001, 0.01, 0.05\}$ | $n = 500$ $m = 30$ $\alpha = 0.001$ |
| Linear SVM (SVM-Lin) | Regularization (C) | $C = \{1, 10, 100, 1000\}$ | $C = 100$ |
| Gaussian-kernel SVM (SVM-RBF) | Regularization (C) Kernel coefficient (γ) | $C = \{1, 10, 100, 1000\}$ $\gamma = \{1, 10, 100, 1000\}$ | $C = 100$ $\gamma = 10$ |
| Adaboost classifier (ABC) | Estimators (n) Maximum depth (m) Learning rate (α) | $n = \{100, 200, \dots 1000\}$ $m = \{10, 20, \dots 100\}$ $\alpha = \{0.0001, 0.001, 0.01, 0.05\}$ | $n = 200$ $m = 20$ $\alpha = 0.01$ |
| Gaussian process classifier (GPC) | Kernel (K) | $K = \text{RBF}$ | $K = \text{RBF}$ |
| DT | Maximum depth (m) Pruning (p) | $m = \{10, 20, \dots 100\}$ $p = \{2, 4, 6, 8, 10, 12\}$ | $m = 50$ $p = 12$ |
| KNN | Number of neighbours (k) Weight function (w) | $k = \{1, 2, 3, \dots 100\}$ $w = \{\text{uniform, distance}\}$ | $k = 5$ $w = \text{uniform}$ |
| MLP classifier | Number of Layers (h) Number of nodes (a) Activation function (f) Learning rate (α) | $h = 1$ $a = \{70, 35, 14, 7, 1\}$ $f = \{\text{Tanh, ReLU, Logistic, Sigmoid}\}$ $\alpha = \{0.0001, 0.001, 0.01, 0.05\}$ | $a = 7$ $f = \text{ReLU}$ $\alpha = 0.001$ |
| DNN classifier | Number of Layers (h) Number of nodes (a) Activation function (f) Learning rate (α) | $h = \{2, 3\}$ $a = \{(70, 35, 14), (70, 14, 35), (35, 70, 14), (35, 14, 70), (70, 35), (35, 70), (70, 14), (14, 70), (35, 14), (14, 35)\}$ $f = \{\text{Tanh, ReLU, Logistic, Sigmoid}\}$ $\alpha = \{0.0001, 0.001, 0.01, 0.05\}$ | $h = 3$ $a = (35, 70, 14)$ $f = \text{ReLU}$ $\alpha = 0.001$ |
| Naive Bayes classifier (NBC) | Gaussian | – | – |
| Quadratic discriminant analysis (QDA) | Regularization strength inverse (C) | $C = \{0.001, 0.01, 0.1, 1, 10, 100, 1000\}$ | $C = 0.01$ |

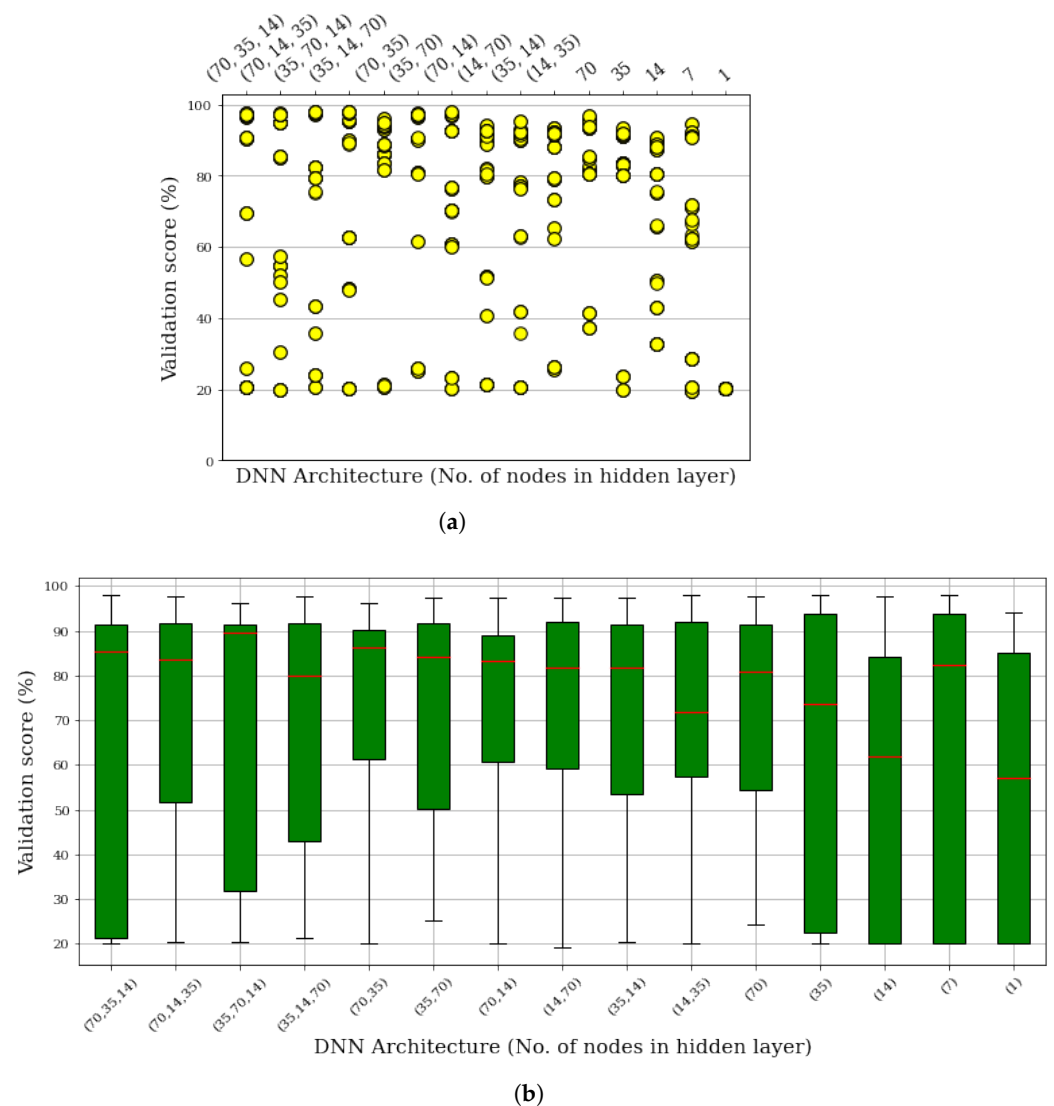


Figure 6. Validation scores of different DNN architectures over a five-fold cross validation. (a) A complete assessment view; (b) boxplot of each DNN architecture's performance.

4.3. Diagnostic Performance Evaluation

Performance metrics for monitoring fault detection and diagnostic systems are well established, including accuracy, precision, sensitivity, recall, F1-score, support, etc. These metrics, at zero false alarm rate, return a value of 1, while at a 100% false prediction, they return a value of zero. Detailed definitions of these metrics can be found in [15]; however, they are calculated from true positives (TP), false positives (FP), false negatives (FN), and true negative (TN) values. In addition to the above evaluation metrics, the hardware computational cost is also another factor worth considering in the choice of diagnostic model acceptance/rejection. This is because some algorithms may have superior predictive capabilities for diagnostics but come with significantly higher computational costs, while others may not be as inexpensive as they are prediction-capable. Therefore, a wider perspective of algorithm reliability assessment ensures that as much as possible, the choice of diagnostic model is backed up by practically acceptable factors.

Following a successful training of the classifiers, the test data were simultaneously deployed on the respective models for testing. Figure 7 shows the comprehensive diagnostic performance evaluation results of the classifiers.

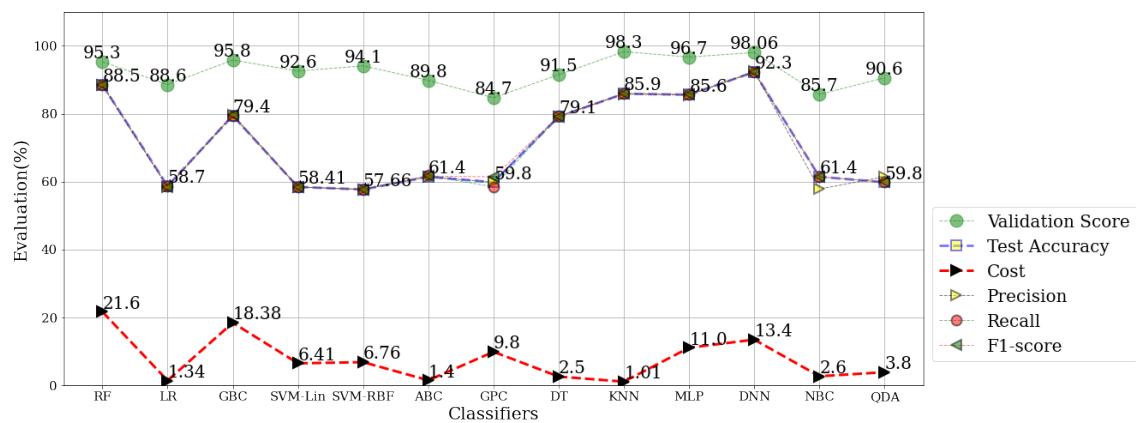


Figure 7. Diagnostics performance (test score) comparison of ML-based classifiers on the test data.

As shown, against high training accuracies (in green dots), the relatively poorer performance of most of the other classifiers can be attributed to their limited efficiencies for highly indiscriminate cases similar to the one presented in this study. In contrast, the superior learning capabilities of the DNN are revealed by the highest test accuracy, precision, recall, and F1-scores. Arguably, the performance of the other classifiers may be further improved (marginally) with other optimization methods apart from the grid search technique; however, this is sure to increase the probability of over-fitting which may not be realistically reliable for safety-critical applications. On the other hand, their respective computational costs presented by the red dotted lines reveal the cost contribution (in percentage, the total training time in seconds) of each algorithm to the whole training time. For reference, all analyses were done in Scikitlearn Python 3.7 library on a desktop computer with the specifications: AMD Ryzen 7 (manufactured in Taiwan), 2700 Eight-core 3.20 GHz processor, and 16 GB RAM.

With a test accuracy of 92.3% from the DNN model, it is clear that increasing the number of layers of an MLP to form a DNN enhances its learning and predictive capabilities; however, the lower costs (85.6%) of the MLP in comparison with the DNN's cost (13.4%) allow us to verify the cost implications of the DNN initiative. Overall, the RF ranks second to the DNN with a test score of 88.5%; however, since it is clearly the most expensive (with a computational cost of 21.6%) and is naturally affected by high dimensional inputs and noise, its reliability for practical use remains questionable. Sadly, the SVM variants (SVM-Lin and SVM-RBF, respectively) were the least effective with test accuracies of 58.41% and 57.66%, respectively.

4.4. Discussions and Drawn Insights

The results reported so far reveal the robustness of the wavelet transform and DNN for CRD FIS monitoring/diagnostics under W/D emulsion conditions alongside an investigative discussion on the water-induced damage severity on critical injector components. These results are expected to support the campaign for greener energy, emission and cost reduction, and environmental health by fuel emulsification. Although all hopes seem high when only the benefits are considered, the inherent wear/oxidation (long-term) effects from diesel emulsification may impede on-going plans (if any exist) for global adoption. Contrary to diesel emulsification, engine downsizing also seems like a promising solution; nonetheless, achieving a globally acceptable engine design on which costs, environmental concerns, wear issues, etc., are well addressed seems impossible since the realization of one may imply forfeiting the other(s) [21].

While the empirical validations presented herein support the proposed methodology, it is important to highlight that three major challenges affect the usability of CR pressure signals for condition monitoring—the non-stationarity of the signals, choice of wavelet, and uncertainties. Interestingly, computing the first-order time-dependent derivatives of the signals not only stationarizes the signals but also provides an unbiased standpoint for

extracting discriminative features for diagnosis/FDI. On the other hand, recent solutions on uncertainty modeling (when properly harnessed) may offer reliable solutions [43]. Particularly for wavelet choice, it may be exhaustive to discover an optimal wavelet considering the numerous wavelets (and their variants) available for exploration; however, non-complex wavelets offer a reliable kick-start to choose from (if the E-SER approach seems time-consuming/computationally expensive).

Particularly for the proposed DNN classifier, it can be observed from the test performance (confusion matrix) presented in Figure 8 that the model's class-specific prediction performance was quite reliable considering the significant inter-class similarities in the emulsions and varying engine speeds.

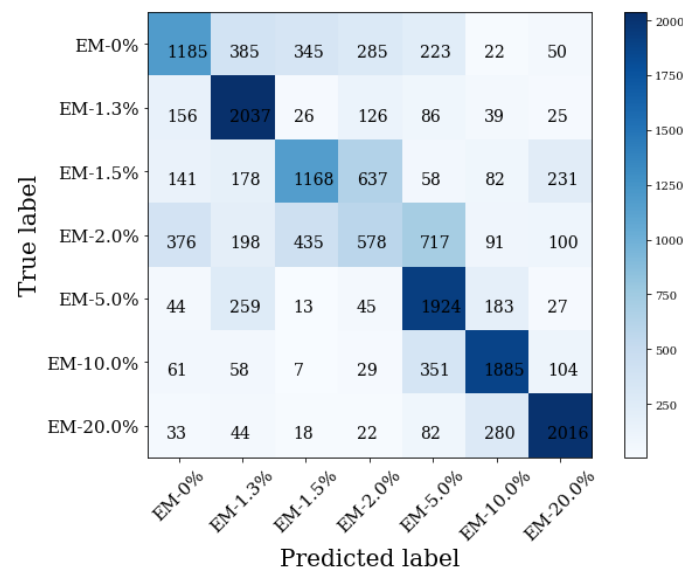


Figure 8. Class-specific diagnostics performance by DNN: confusion matrix.

As shown in Figure 8, 717 inputs from EM-2% were wrongly classified as EM-5%, whereas only 578 samples were accurately classified. This implies that most EM-2% CWCs have a high similarity with EM-5%; however, a look at the other classes will reveal reliable diagnosis outputs, with EM-1.3% and EM-20% being the most accurately diagnosed with 2037 and 2016 TPs, respectively. From a different perspective, it can be observed that from EM-5% to EM-20%, the false alarm rate of detection is significantly reduced. This implies that the impact of these excessive water compositions in diesel is quite significant and can be easily detected by the diagnostic model. As much as the model was able to diagnose all the classes (emulsion compositions) reliably, as observed, with relatively few FNs and FPs for each class except EM-2%, the proposed framework is validated.

5. Concluding Remarks

Although existing studies reveal encouraging paradigms for the use of water-emulsified diesel fuels for improved fuel efficiency and a more eco-friendly environment, the reliability of such methods remains open for continued discussions. Issues of stability, mixing conditions, temperature, and mixing compositions greatly influence the reliability of water-emulsified diesel fuels; however, this study proposes the use of CR system characteristics for drawing valid conclusions on a safe emulsion composition for the commercial diesel-fuel engine. The presented experimental studies suggest that beyond a water-emulsion composition of 10% water by volume of emulsion, the reliability of the emulsified fuel for optimum engine efficiency is threatened.

From the investigative assessments presented in the study, a reliable ML-based diagnostics scheme was proposed and validated on the RPS signals across various water-in-diesel emulsions at various engine speeds. This diagnostic framework functions on the

assumption that the standardized first-order differentials of CR pressure signals not only eliminate the issues of nonstationarity in the inputs, but they also provide reliable discriminative properties for use by wavelet transform which returns discriminative spectral and transient information for diagnosis. The results show that by extracting the CWCs from the first-order differentials up to the 512th scale on a Mexican hat wavelet, adequate fault parameters can be extracted from which highly salient features can be selected for use by the DNN classifier whose hyperparameters were globally optimized. With a test accuracy of 92.3% against other widely-used ML-based diagnostic tools, the proposed DNN-based diagnostics tool was empirically assessed using several performance evaluation metrics.

Although the study presented here was validated with strong arguments, its potential for improvement remains healthy for continued research. For instance, the impact of feature-selection techniques for improved diagnostics accuracy and computational costs were only considered from a correlation-based perspective only. Obviously, the numerous wrapper-based and hybrid methods still remain unexplored, and this could motivate continued research paths for investigation. From a deeper perspective, because passive control improves a diagnostics scheme (since the W/D emulsions were pre-designed) while introducing more conservativeness, online performance is limited. Therefore, continued research studies would be aimed at exploring real-time diagnostic solutions while considering costs and interpretability for industrial applicability.

Author Contributions: Conceptualization, U.E.A.; methodology, U.E.A.; software, U.E.A.; formal analysis, U.E.A.; investigation, U.E.A.; resources, U.E.A. and J.-W.H.; data curation, U.E.A.; writing—original draft, U.E.A.; writing—review and editing, U.E.A. and J.-W.H.; visualization, U.E.A.; supervision, J.-W.H.; project administration, J.-W.H.; funding acquisition, J.-W.H. All authors have read and agreed to the published version of the manuscript.

Funding: This research was supported by the MSIT (Ministry of Science and ICT), Korea, under the Grand Information Technology Research Center support program (IITP-2020-2020-0-01612) supervised by the IITP (Institute for Information & Communications Technology Planning & Evaluation).

Institutional Review Board Statement: Not applicable.

Informed Consent Statement: Not applicable.

Data Availability Statement: The data presented in this study are available on request from the corresponding author. The data are not publicly available due to laboratory regulations.

Acknowledgments: Early preliminary research was supported by Mr. Min Seop Kim affiliated with the Department of Mechanical Engineering (Department of Aeronautics, Mechanical and Electronic Convergence Engineering), Kumoh National Institute of Technology.

Conflicts of Interest: The authors declare no conflict of interest.

Appendix A. Damage Severity Analysis on Injector Components

Ideally, the smooth reciprocating movement of the plunger in a fuel injector of a CRD engine relies on little/no friction between the plunger and the valve, which under realistic conditions is ensured by the lubricating effect and low viscosity of diesel. Unfortunately, W/D emulsions increase the viscosity values of the fuel which results in higher friction between reciprocating components in the injector [21]. In addition, the water molecules induce oxidation of the metal components which further results in corrosion, increased friction, and inevitably, component wear.

Following a back-leak test and microscopic analysis of the injectors after conducting the W/D emulsion test on the cases study, Figures A1–A3 reveal, respectively, the water-induced wear severity on the injector pistons, needles, and ball seats, respectively.

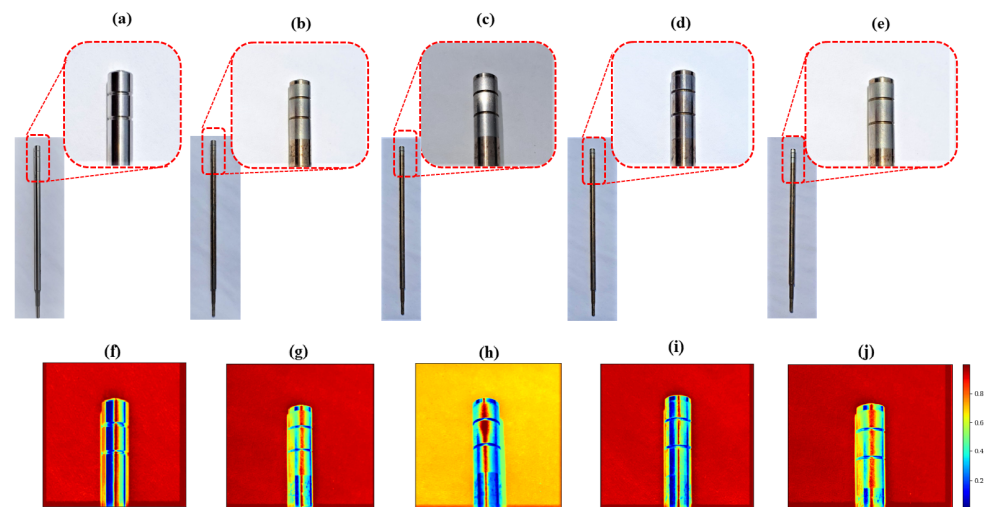


Figure A1. Comparison of injector valve pistons between (a) normal injector, (b–e) the worn injectors after the experiment, and (f–j) the surface profiles for the respective injector valve pistons.

Contrary to the normal injector valve piston shown in Figure A1a–j reveal that injector valve pistons were worn as a result of the W/D emulsion fuels; these are highlighted in red rectangles. Figure A2b–e,g–j also reveal the wear effects of the W/D emulsions on the injector needles in comparison with a normal needle (see Figure A2a).

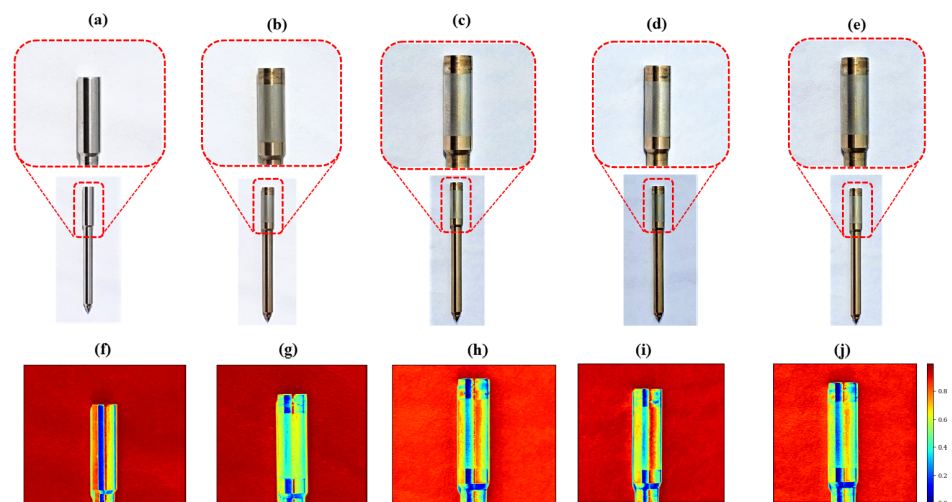


Figure A2. Comparison of injector nozzle needles between (a) normal injector, (b–e) the worn injectors after the experiment, and (f–j) the surface profiles for the respective injector valve pistons.

Observing the piston valves in Figure A2b–e,g–j better reveals the wear effects compared to the normal needle in Figure A2a,f. In addition, a microscopic observation of the valve ball seat shows in Figure A3 the oxidation/corrosion effects of the W/D emulsions on them.

Unlike in Figure A3a,f which shows a smooth circumference (and non-oxidized nature) of the ball seat edge of a normal injector valve ball seat, the whiteness (highlighted in red circles) and roughness of the ball seat edges in Figure A3b–e,g–j reveals the oxidation/corrosion effect of the W/D emulsion fuels.

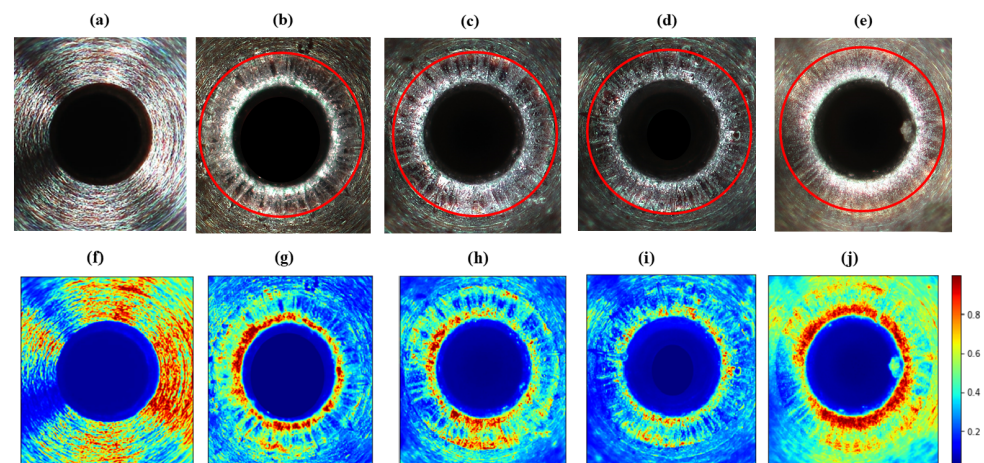


Figure A3. Comparison of injector valve ball seats between (a) normal injector, (b–e) the worn injectors after the experiment, and (f–j) the surface profiles for the respective injector valve pistons.

References

- Krogerus, T.; Huhtala, K. Diagnostics and Identification of Injection Duration of Common Rail Diesel Injectors. *Open Eng.* **2018**, *8*, 1–6. [[CrossRef](#)]
- Liang, J.; Zhang, Q.; Chen, Z.; Zheng, Z.; Yang, C.; Ma, Q. The combustion and emission characteristics of diesel-ethanol blends with THF as cosolvents in a diesel engine operating with EGR. *Fuel* **2021**, *298*, 120834. [[CrossRef](#)]
- Krishnamoorthi, M.; Malayalamurthi, R. The influence of charge air temperature and exhaust gas recirculation on the availability analysis, performance and emission behavior of diesel-bael oil-diethyl ether blend operated diesel engine. *J. Mech. Sci. Technol.* **2018**, *32*, 1835–1847. [[CrossRef](#)]
- Kalghatgi, G.; Johansson, B. Gasoline compression ignition approach to efficient, clean and affordable future engines. *Proc. Inst. Mech. Eng. Part D J. Automob. Eng.* **2018**, *232*, 118–138. [[CrossRef](#)]
- Senthur, N.S.; BalaMurugan, S.; RamGanesh, H.; Divakara, S. Experimental analysis on the performance, emission, and combustion characteristics of diesel, and diesel-water emulsions in low heat rejection engine. *Mater. Today Proc.* **2021**, *39*, 1351–1355. [[CrossRef](#)]
- Won, J.; Baek, S.W.; Kim, H.; Lee, H. The Viscosity and Combustion Characteristics of Single-Droplet Water-Diesel Emulsion. *Energies* **2019**, *12*, 1963. [[CrossRef](#)]
- Khatri, D.; Goyal, R. Performance, emission and combustion characteristics of water diesel emulsified fuel for diesel engine: A review. *Mater. Today Proc.* **2020**, *28*, 2275–2278. [[CrossRef](#)]
- Hussain, V.R.; Marouf, W.M. Optimal utilization of ZnO nanoparticles blended diesel-water emulsion by varying compression ratio of a VCR diesel engine. *J. Environ. Chem. Eng.* **2020**, *2020*, 103884. [[CrossRef](#)]
- Hossain, F.M.; Nabi, M.N.; Rahman, M.M.; Bari, S.; Van, T.C.; Rahman, S.M.A.; Rainey, T.J.; Bodisco, T.A.; Suara, K.; Ristovski, Z.; et al. Experimental Investigation of Diesel Engine Performance, Combustion and Emissions Using a Novel Series of Dioctyl Phthalate (DOP) Biofuels Derived from Microalgae. *Energies* **2019**, *12*, 1964. [[CrossRef](#)]
- Avulapati, M.M.; Megaritis, T.; Xia, J.; Ganippa, L. Experimental understanding on the dynamics of micro-explosion and puffing in ternary emulsion droplets. *Fuel* **2019**, *239*, 1284–1292. [[CrossRef](#)]
- Song, E.; Ke, Y.; Yao, C.; Dong, Q.; Yang, L. Fault Diagnosis Method for High-Pressure Common Rail Injector Based on IFOA-VMD and Hierarchical Dispersion Entropy. *Entropy* **2019**, *21*, 923. [[CrossRef](#)]
- Akpudo, U.E.; Hur, J.W. Towards bearing failure prognostics: A practical comparison between data-driven methods for industrial applications. *J. Mech. Sci. Technol.* **2020**, *34*, 4161–4172. [[CrossRef](#)]
- Akpudo, U.E.; Hur, J.W. A feature fusion-based prognostics approach for rolling element bearings. *J. Mech. Sci. Technol.* **2020**, *34*, 4025–4035. [[CrossRef](#)]
- Nixon, S.; Weichel, R.; Reichard, K.; Kozlowski, J. A Machine Learning Approach to Diesel Engine Health Prognostics using Engine Controller Data. In Proceedings of the 10th Annual Conference of the Prognostics and Health Management Society, Philadelphia, PA, USA, 24–27 September 2018; Volume 10. [[CrossRef](#)]
- Akpudo, U.; Jang-Wook, H. A Multi-Domain Diagnostics Approach for Solenoid Pumps Based on Discriminative Features. *IEEE Access* **2020**, *8*, 175020–175034. [[CrossRef](#)]
- Visalakshi, S.; Radha, V. A literature review of feature selection techniques and applications: Review of feature selection in data mining. In Proceedings of the the 2014 IEEE International Conference on Computational Intelligence and Computing Research, Coimbatore, India, 18–20 December 2014; pp. 1–6.
- Syu, J.Y.; Chang, Y.Y.; Tseng, C.H.; Yan, Y.L.; Chang, Y.M.; Chen, C.C.; Lin, W.Y. Effects of water-emulsified fuel on a diesel engine generator's thermal efficiency and exhaust. *J. Air Waste Manag. Assoc.* **2014**, *64*, 970–978. [[CrossRef](#)]

18. Senthur, N.S.; Jose, V.J.; Mahesh, K.M.; Esakki, R.M. Relative assessment of performance and emission characteristics of various biodiesel water emulsion blends in DI diesel engine. *Mater. Today Proc.* **2021**, *45*, 967–973. [[CrossRef](#)]
19. Fahd, M.E.A.; Wenming, Y.; Lee, P.S.; Chou, S.K.; Yap, C.R. Experimental investigation of the performance and emission characteristics of direct injection diesel engine by water emulsion diesel under varying engine load condition. *Appl. Energy* **2013**, *102*, 1042–1049. [[CrossRef](#)]
20. Kim, M.; Oh, J.; Lee, C. Study on Combustion and Emission Characteristics of Marine Diesel Oil and Water-In-Oil Emulsified Marine Diesel Oil. *Energies* **2018**, *11*, 1830. [[CrossRef](#)]
21. Kim, M.-S.; Akpudo, U.E.; Hur, J.-W. A Study on Water-Induced Damage Severity on Diesel Engine Injection System Using Emulsified Diesel Fuels. *Electronics* **2021**, *10*, 2285. [[CrossRef](#)]
22. Patidar, S.K.; Raheman, H. Performance and durability analysis of a single-cylinder direct injection diesel engine operated with water emulsified biodiesel-diesel fuel blend. *Fuel* **2020**, *273*, 117779. [[CrossRef](#)]
23. Turner, J.; Popplewell, A.; Patel, R.; Johnson, T.; Darnton, N.J.; Richardson, S.; Bredda, S.W.; Tudor, R.J.; Bithell, C.I.; Jackson, R.; et al. Ultra Boost for Economy: Extending the Limits of Extreme Engine Downsizing. *SAE Int. J. Engines* **2014**, *7*, 387–417. [[CrossRef](#)]
24. Serrano, J.R.; Novella, R.; Piqueras, P. Why the Development of Internal Combustion Engines Is Still Necessary to Fight against Global Climate Change from the Perspective of Transportation. *Appl. Sci.* **2019**, *9*, 4597. [[CrossRef](#)]
25. Beatrice, C.; Di Blasio, G.; Belgiorno, G. Experimental analysis of functional requirements to exceed the 100kW/l in high-speed light-duty diesel engines. *Fuel* **2017**, *207*, 591–601. [[CrossRef](#)]
26. Di Blasio, G.; Beatrice, C.; Belgiorno, G.; Pesce, F.C.; Vassallo, A. Functional Requirements to Exceed the 100 kW/l Milestone for High Power Density Automotive Diesel Engines. *SAE Int. J. Engines* **2017**, *10*, 2342–2353. [[CrossRef](#)]
27. Vassallo, A.; Beatrice, C.; Di Blasio, G.; Belgiorno, G.; Avolio, G.; Pesce, F.C. *The Key Role of Advanced, Flexible Fuel Injection Systems to Match the Future CO₂ Targets in an Ultra-Light Mid-Size Diesel Engine*; SAE Technical Paper; SAE International: Washington, DC, USA, 2018; ISSN: 0148-7191. [[CrossRef](#)]
28. Wróblewski, A.; Langer, A.; Szczyglak, P.; Rekuć, A. The Influence of Added Water on Fuel Injector Wear in a Diesel Engine. *Tribologia* **2018**, *3*, 153–158. [[CrossRef](#)]
29. Nour, M.; Kosaka, H.; Ali, K.; Abdel-Rahman; Bady, M. Effect of Water Injection into Exhaust Manifold on Diesel Engine Combustion and Emissions. *Energy Procedia* **2016**, *100*, 178–187. [[CrossRef](#)]
30. Suresh, V.; Amirthagadeswaran, K.S. The role of water-in-diesel emulsion and its additives on diesel engine performance and emission levels: A retrospective review. *Alex. Eng. J.* **2016**, *55*, 2463–2472. [[CrossRef](#)]
31. Shyam, P.H.; Gonsalvis, J.; Vijay, V.S. Effect of Introduction of Water into Combustion Chamber of Diesel Engines—A Review. *Energy Power* **2015**, *5*, 28–33. [[CrossRef](#)]
32. Kim, S.; Akpudo, U.E.; Hur, J.-W. A Cost-Aware DNN-Based FDI Technology for Solenoid Pumps. *Electronics* **2021**, *10*, 2323. [[CrossRef](#)]
33. Akpudo, U.E.; Hur, J.-W. D-dCNN: A Novel Hybrid Deep Learning-Based Tool for Vibration-Based Diagnostics. *Energies* **2021**, *14*, 5286. [[CrossRef](#)]
34. Akpudo, U.E.; Hur, J.-W. A CEEMDAN-Assisted Deep Learning Model for the RUL Estimation of Solenoid Pumps. *Electronics* **2021**, *10*, 2054. [[CrossRef](#)]
35. Chen, X.; Yang, Y.; Cui, Z.; Shen, J. Wavelet Denoising for the Vibration Signals of Wind Turbines Based on Variational Mode Decomposition and Multiscale Permutation Entropy. *IEEE Access* **2020**, *8*, 40347–40356. [[CrossRef](#)]
36. Akpudo, U.E.; Hur, J. A Cost-Efficient MFCC-Based Fault Detection and Isolation Technology for Electromagnetic Pumps. *Electronics* **2021**, *10*, 439. [[CrossRef](#)]
37. Han, T.; Jiang, D.; Zhao, Q.; Wang, L.; Yin, K. Comparison of random forest, artificial neural networks and support vector machine for intelligent diagnosis of rotating machinery. *Trans. Inst. Meas. Control* **2018**, *40*, 2681–2693. [[CrossRef](#)]
38. Khaire U.M.; Dhanalakshmi, R. Stability of feature selection algorithm: A review. *J. King Saud Univ.-Comput. Inf. Sci.* **2019**, ISSN 1319-1578. [[CrossRef](#)]
39. Lai, K.K.; Mishra, S.K.; Ram, B. On q-Quasi-Newton's Method for Unconstrained Multiobjective Optimization Problems. *Mathematics* **2020**, *8*, 616. [[CrossRef](#)]
40. Kingma, D.P.; Ba, J. Adam: A Method for Stochastic Optimization. *arXiv* **2015**, arXiv:1412.6980v9.
41. Oh, S.H. Improving the Water Level Prediction of Multi-Layer Perceptron with a Modified Error Function. *Int. J. Contents* **2018**, *13*, 23–28. [[CrossRef](#)]
42. Bircanoğlu, C.; Arica, N. A comparison of activation functions in artificial neural networks. In Proceedings of the 2018 26th Signal Processing and Communications Applications Conference (SIU), Izmir, Turkey, 2–5 May 2018; pp. 1–4. [[CrossRef](#)]
43. Chatzimichail, T.; Hatjimihail, A.T. A Software Tool for Calculating the Uncertainty of Diagnostic Accuracy Measures. *Diagnostics* **2021**, *11*, 406. [[CrossRef](#)]